Microstructured Surfaces for Reducing Chances of Fomite Transmission via Virus-Containing Respiratory Droplets

Citation: Kim, Seok et al. "Microstructured Surfaces for Reducing Chances of Fomite Transmission via Virus-Containing Respiratory Droplets." ACS Nano 15, 9 (August 2021): 14049–14060. © 2021 The Authors

As Published: http://dx.doi.org/10.1021/acsnano.1c01636

Publisher: American Chemical Society (ACS)

Persistent URL: https://hdl.handle.net/1721.1/132715

Version: Final published version: final published article, as it appeared in a journal, conference proceedings, or other formally published context

ACS NANO

www.acsnano.org

ARTICLE

Microstructured Surfaces for Reducing Chances of Fomite Transmission via Virus-Containing Respiratory Droplets

Seok Kim, Woo Young Kim, Sang-Hoon Nam, Seunghang Shin, Su Hyun Choi, Do Hyeog Kim, Heedoo Lee, Hyeok Jae Choi, Eungman Lee, Jung-Hyun Park, Inho Jo, Nicholas X. Fang, and Young Tae Cho*

Cite This: *ACS Nano* 2021, 15, 14049–14060

Read Online

ACCESS | Metrics & More | Article Recommendations | Supporting Information

ABSTRACT: **Evaporation-induced particle aggregation in drying droplets is of significant importance in the prevention of pathogen transfer due to the possibility of indirect fomite transmission of the infectious virus particles. In this study, particle aggregation was directionally controlled using contact line dynamics (pinned or slipping) and geometrical gradients on microstructured surfaces by the systematic investigation of the evaporation process on sessile droplets and sprayed microdroplets laden with virus-simulant nanoparticles. Using this mechanism, we designed robust particle capture surfaces by significantly inhibiting the contact transfer of particles from fomite surfaces. For the proof-of-concept, interconnected hexagonal and inverted pyramidal microwall were fabricated using ultraviolet-based nanoimprint lithography, which is considered to be a promising scalable manufacturing process. We demonstrated the potentials of an engineered microcavity surface to limit the contact transfer of particle aggregates deposited with the evaporation of microdroplets by 93% for hexagonal microwall and by 96% for inverted pyramidal microwall. The particle capture potential of the interconnected microstructures was also investigated using biological particles, including adenoviruses and lung-derived extracellular vesicles. The findings indicate that the proposed microstructured surfaces can reduce the indirect fomite transmission of highly infectious agents, including norovirus, rotavirus, or SARS-CoV-2, via respiratory droplets.**

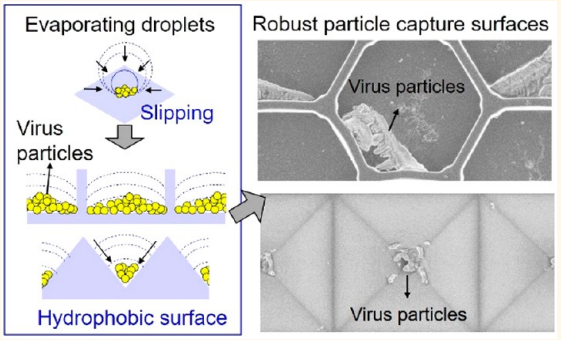

KEYWORDS: *microstructured surfaces, respiratory droplets, nanoparticles, virus particles, fomite transmission, directional particle aggregation*

INTRODUCTION

According to WHO, highly infectious diseases can be transmitted via contact, droplets, air, fomites, and blood, via the fecal−oral, from mother to child, and from animal to human transmission.[1,2] Since viruses, including SARS-CoV-2, can survive on contaminated surfaces and objects (fomites) on which respiratory droplets from infected individuals have been expelled,[3,4] indirect fomite transmission contributes to the spread of many enteric and some respiratory pathogens.[2,3,5−7] Moreover, recent studies have shown that viruses can survive on surfaces from several hours to several weeks, especially in areas with close contact and high-touch surfaces, such as airplanes or hospitals.[8−10] The surface stability of viruses may promote fomite transmission and exacerbate other health issues in conjunction with other existing pathogens, and overall, this may exert a significant impact on human health.[11] Although there is limited evidence of fomite transmission in SARS-CoV-2,[12] transmission through fomites should be considered a risk factor in the spread of respiratory and enteric viral diseases, including SARS-CoV-2, because of consistent results showing environmental contamination with the identification of pathogenic organisms.[1,2,13] Moreover, human touch may significantly influence the risk of infection and disease spread via the fomite route.[15,16] Accordingly, it is critical to develop approaches to

Received: February 23, 2021
Accepted: July 23, 2021
Published: August 2, 2021

https://doi.org/10.1021/acsnano.1c01636
ACS Nano 2021, 15, 14049−14060

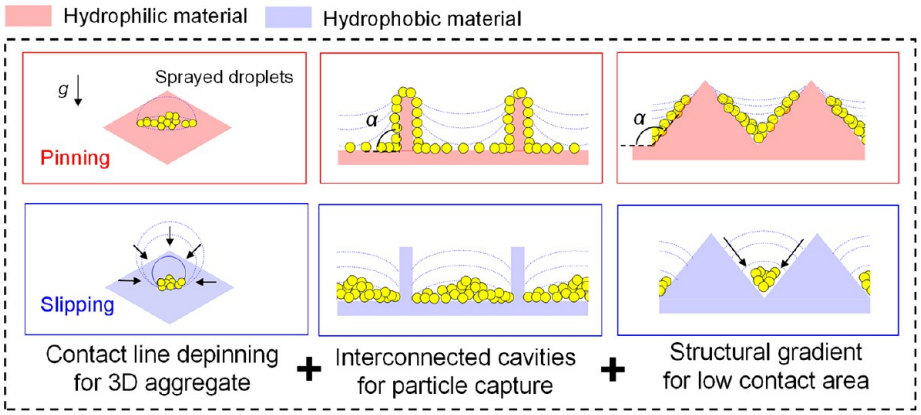

Figure 1. Design of robust particle capture surfaces to reduce contact transfer from contaminated surfaces. The topography of the interconnected microcavity was designed to improve the structural stability of the microstructures and robustness of particle capture after deposition of the respiratory microdroplets. We further designed the microcavity to include an asymmetric slope for the directional transport of microdroplets during spontaneous evaporation caused by capillary force and contact angle hysteresis (CAH) and an ultralow solid contact area.

disrupt the fomite transmission of highly infectious disease-causing agents on contaminated surfaces.

Despite the potential importance of indirect fomite transmission, only a limited number of studies have been conducted on the desired surfaces and surface technologies that can help reduce fomite transmission via contaminated surfaces and objects effectively. In particular, a low touch transfer from preinfected objects (e.g., mimicking hand contact) to microstructured surfaces is demonstrated in the previous studies.[11,17] For instance, Imani et al. suggested that engineered surfaces effectively reduce the adhesion, proliferation, and transfer of bacteria to a hierarchical surface with small areas due to the rough nature of the surface, resulting in a low adhesive force for bacterial attachment.[17] Li and co-workers demonstrated a bead transfer method for evaluating indirect fomite transmission from pathogen-contaminated objects to microstructured surfaces.[11] The micropatterned surfaces with a reduced surface area of contact for pathogens limited the transmission of model bacteria, phages, and human viruses. However, these studies described only the antibacterial or antiviral effect of microstructured surfaces caused by a small contact area. To date, fomite-based transmission from microstructured surfaces with virus particles deposited by respiratory droplets or aerosols to other clean surfaces or skin (e.g., hands) has not been well characterized.

In this study, we designed a robust microstructured surface to control particle aggregation for facilitating low transmission from fomite surfaces, which can help reduce the chances of contact infection by various virus particles (VPs) via respiratory droplets. As the first component of our surface design, the microstructure consisted of an interconnected cavity with a low contact area that captured the particles, which could help prevent high-touch surface contamination in the healthcare environment. The interconnected microcavity architecture also enhanced the mechanical robustness, as observed for various natural structures including springtail skin and honeycomb,[14,18−20] and maintained the robust particle capture stability from external mechanical contact. Additional design features were considered to ensure directional particle aggregates driven by low contact angle hysteresis (CAH) of the droplets and structural gradient of surfaces to minimize particle residues for extremely low touch transfer. Three experiments were conducted to study the inhibitory effects exerted by the micropatterned surface on particle transmission. First, we investigated the effects of wettability on the evaporation process between the sessile droplets and sprayed microdroplets with suspended nanoparticles. Second, we studied particle aggregation on 3D microstructured surfaces to understand the mechanism underlying directional particle capture. We demonstrated the high particle capture efficacy against mechanical contact transfer. Third, to simulate the deposition of respiratory microdroplets containing infectious VPs, we induced an accumulation of the adenovirus and biological nanoparticles on 3D microstructured surfaces. The fabricated microstructured surfaces can be useful for developing risk reduction strategies for the indirect surface transmission of agents causing infectious disease.

RESULTS AND DISCUSSION

The aerosolized microdroplets containing VPs evaporate and form a residue on surfaces to form fomites. The residue formation process differs based on the process of microdroplet evaporation and particle aggregation in the droplets depending on the wettability and structure of the contaminated surface, which may significantly affect indirect fomite transmission. For surface designing, we considered the structural stability and robust particle capture ability of the surface for high-touch environmental applications, as presented in Figure 1. On the basis of a surface topography inspired by the structure of natural surfaces,[14,18−21] we proposed the design of interconnected microcavity architectures to enhance the mechanical robustness of the microstructures while entrapping the particles within their cavity from external mechanical contact. We developed a V-shaped microcavity as an additional design feature to ensure the insertion of the directional particle aggregates into the microcavities driven by contact line depinning and the low CAH of the evaporating droplets (related to surface chemistry θ_Y). Inspired by the directional liquid dynamics of natural creature structures,[24] we expected that the interconnected V-shaped microcavity could reveal the characteristics of directional particle aggregation. The V-shaped cavities merge the droplets based on the cavity and spatial confinement and mediate a spontaneous transport of the evaporating droplets based on the effect of contact angle hysteresis and capillary force.[24−26] Combining interconnected microcavity and V-shaped structures, we suggested inverted pyramidal interconnected micro-

https://doi.org/10.1021/acsnano.1c01636
ACS Nano 2021, 15, 14049−14060

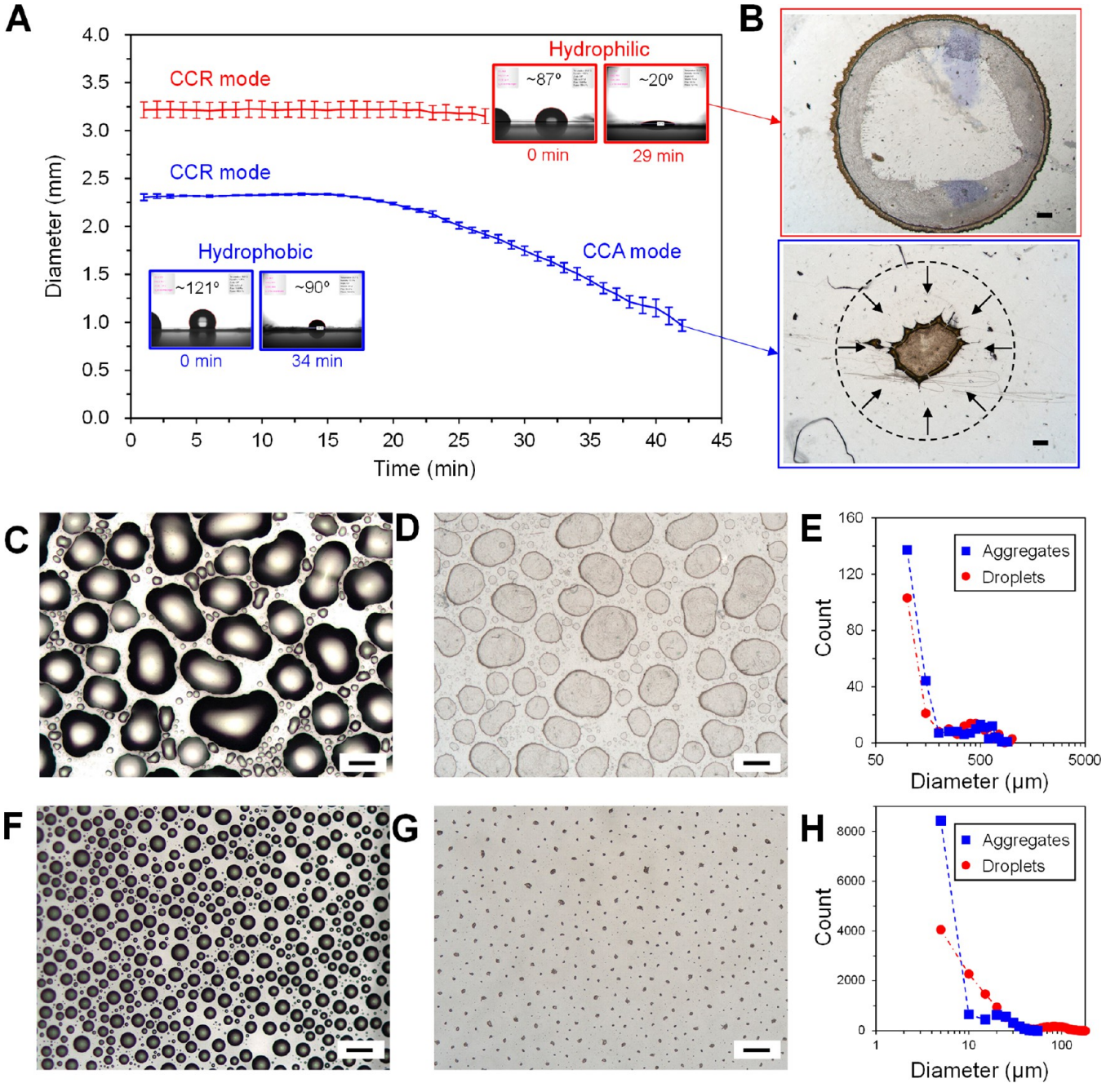

Figure 2. Effect of wettability on the evaporation process, and the particle aggregates in the sessile droplet and sprayed microdroplets. (A) Evolution of contact diameter versus time (n = 3). (B) Particle aggregation in the sessile droplet. Sprayed microdroplets and the resulting particle aggregation; hydrophilic (C, D) and hydrophobic surfaces (F, G). Measured size distribution of sprayed droplets and particle aggregates on hydrophilic (E) and hydrophobic surfaces (H). All scale bars represent 200 μm.

cavities for directional particle aggregation in this study. Furthermore, increasing the structural gradient, which is the angle α between the sidewall and the microcavity substrates, strengthens the mechanical stability of the microstructures from the viewpoint of structural mechanics,[14] which boosts the directional particle aggregation and reduces the solid contact area to minimize touch transfer of contaminated particles.

To assess the effects of surface wettability on particle aggregation, we first investigated the evaporation process of sessile and sprayed droplets laden with nanoparticles on the planar surfaces with different wettability, which correlated with the particle aggregate formation. We used virus-simulant nanoparticles with a mean diameter of 200 nm to mimic infectious VPs and readily detect them on the surfaces.[27] The nanoparticles were mixed in deionized (DI) water and diluted to a concentration of ~1.1×10^{11} particles/mL to simulate the viral load in the respiratory fluid of infected human subjects.[22,28] We also note that the particle concentration was considerably high, similar to the maximum levels observed in clinical samples for the easy detection and visualization of particle aggregation on surfaces.[28] Figure 2 shows the evolution of contact diameter versus time and the resulting formation of aggregates from sessile droplets and sprayed microdroplets containing nanoparticles (see Figure S1 for the evolution of contact angle as a

https://doi.org/10.1021/acsnano.1c01636
ACS Nano 2021, 15, 14049−14060

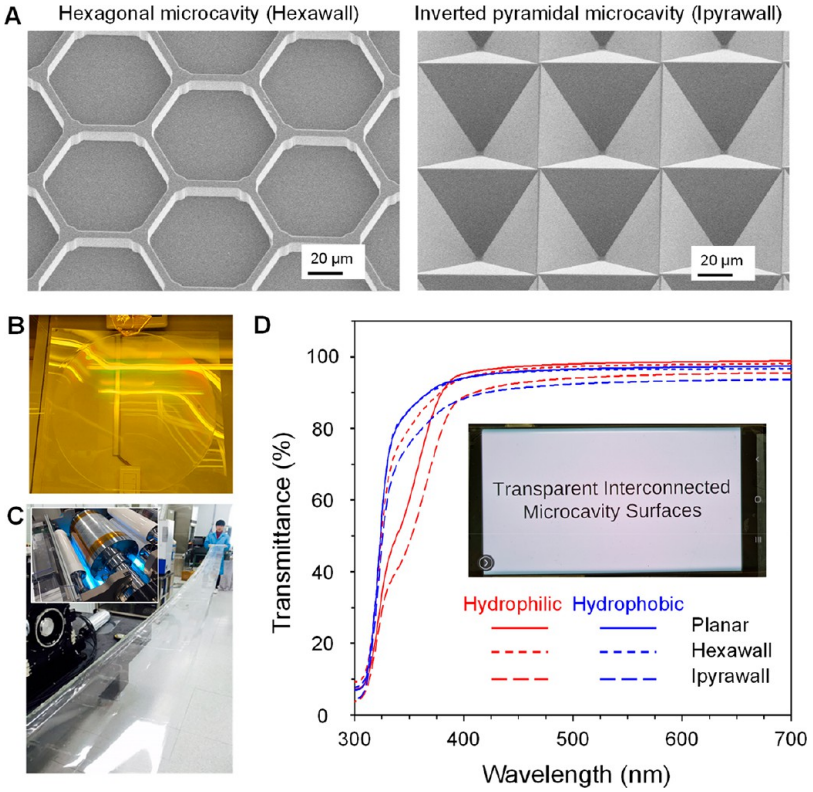

Figure 3. (A) Scanning electron microscope (SEM) image of the imprinted microstructured surfaces. (B) Large-area microstructured surfaces imprinted from 8 in. Si master mold. (C) Currently developing R2R UV imprinting system for high-throughput scalable manufacturing of microstructured surfaces used in this study. (D) Transmission spectra of the interconnected microcavity surfaces. The inlet photograph depicts the transparency of the microcavity surfaces (hexawall), applicable to the touch screen of a smartphone.

function of time). We observed that sessile droplets evaporated in a constant contact radius (CCR, called stick mode) on the hydrophilic planar surface (Young's contact angle θ_Y = ~87°) with pinning at the contact line (Figure 2A), which created a coffee-ring-like stain (Figure 2B). For the hydrophobic planar surface (θ_Y = ~121°), the sessile droplet first evaporated with CCR and then transited to a constant contact angle (CCA, called slip mode) without noticeable pinning at the contact line (Figure 1A), thereby forming a 3D aggregate (Figure 2B). The stick−slip behavior of evaporating particle-laden droplets is attributed to the presence of the nanoparticles,[29] which promotes the pinning of contact lines on both hydrophilic and hydrophobic surfaces (Figure S1). It is reasonable to expect that mechanisms similar to those shown in Figure 2 lead to particle aggregate formation after the evaporation of sprayed microdroplets. As expected, owing to the stick and slip motion of the contact line observed in the sessile droplet, we observed the formation of tiny coffee-ring patterns (Figure 2C,D) and 3D aggregates (Figure 2F,G) on hydrophilic and hydrophobic surfaces after the evaporation of the sprayed microdroplets, respectively. Through the size distribution analysis shown in Figures 2E,H and S2, we confirmed that evaporated microdroplets were more concentrated on the hydrophobic surfaces and that 3D aggregates were deposited in a confined region with randomized shape and size (Figure 2G).

The particle aggregates formed due to the slip mode in the evaporating microdroplets on the planar surfaces can result in a more dramatic difference among the 3D microstructured surfaces. For the proof-of-concept, we designed a hexagonal microwall without a structure gradient (hexawall) and an inverted pyramidal microwall with a structure gradient (ipyrawall), considering the structural requirements described in Figure 1B. Our interconnected hexawall ($\alpha = 90°$) and ipyrawall (α = ~125°) were fabricated through the UV-NIL process (Figure 3A,B and see the "Materials and Methods" section),[18,19] which are highly compatible with the roll-to-roll (R2R) printing[30] for scalable manufacturing of functional surfaces (Figure 3C). Additionally, the transparency of our microcavity surfaces as shown in Figure 3D, is compatible with optical sensing technologies (e.g., surface-enhanced Raman spectroscopy-based biosensor)[33] and other in practical applications (e.g., touch screens).[34]

Figure 4 shows the evaporation process and the particle aggregates of the hexawall surfaces with different wettabilities. For the hydrophilic interconnected hexawall surfaces, the sprayed microdroplets tended to coalesce, which led to the establishment of the typical Wenzel state (Figure 4A). After the evaporation of the sprayed microdroplets, the particles were deposited and aggregated on the top, sides, and bottom of the microcavities owing to the concave-shaped contact line formed by the stick mode on the surfaces (Figure 4B,C). On the hydrophobic interconnected hexawall surfaces, the sprayed droplets remained small microdroplets (Figure 4D). During the evaporation process, the microdroplets tended to be trapped within the microcavity with a convex-shaped contact line (Figure 4F) because of the slip mode of the evaporating droplets on the hydrophobic material, and most particles were deposited and aggregated at the bottom of the microcavity (Figure 4E). The high particle capture efficiency of the microcavity was attributed to the nearly pinning-free surface of the hydrophobic materials, wherein the evaporating droplet could collect almost all particles in the aggregates confined at the bottom.

https://doi.org/10.1021/acsnano.1c01636
ACS Nano 2021, 15, 14049−14060

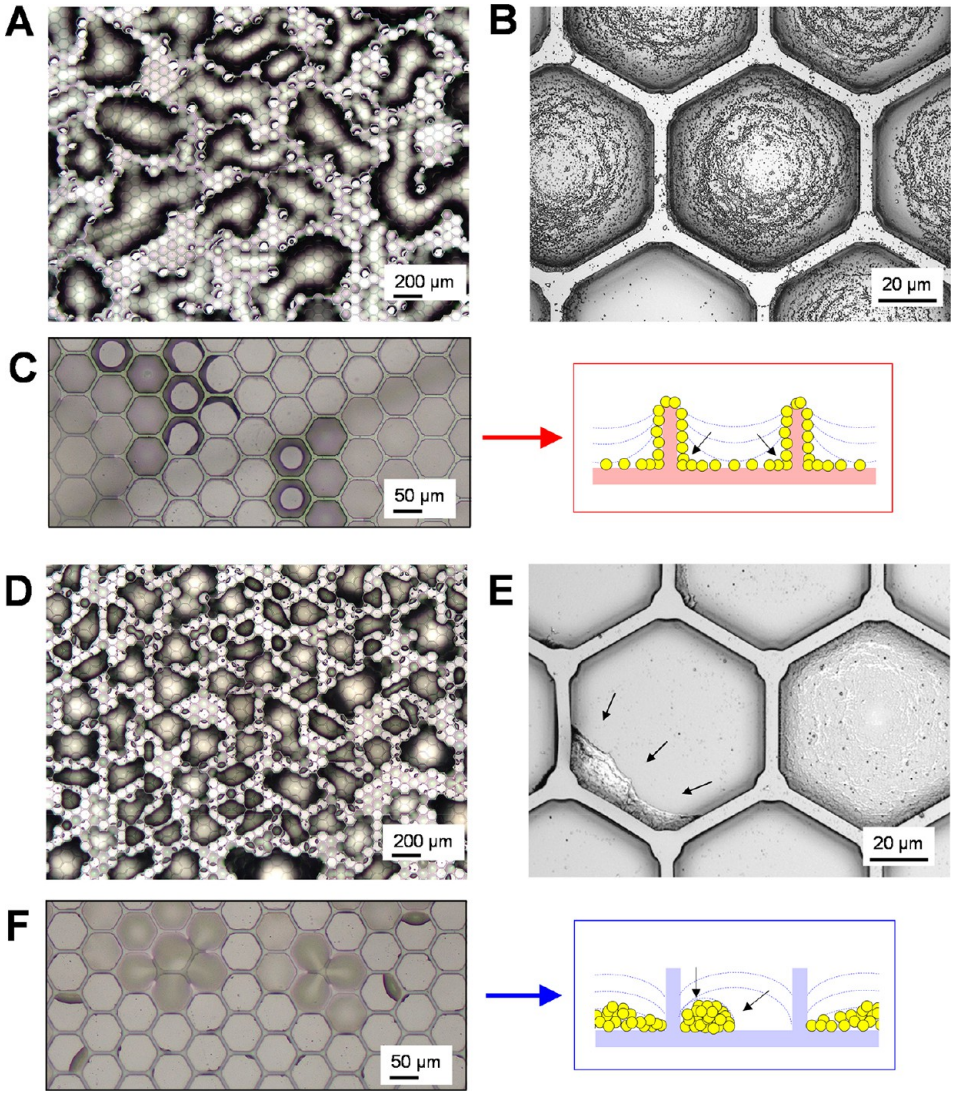

Figure 4. Evaporation process and particle aggregate formations on the hexagonal microwall surfaces (hexawall). (A) Coalescence of sprayed microdroplets. (B) Particle aggregate formation on the hydrophilic hexawall. (C) The evaporating microdroplets formed a concave contact line owing to the pinning on the 3D surfaces. (D) Sprayed microdroplets and (E) particle aggregate formation on the hydrophobic hexawall. (F) The evaporating microdroplets formed a convex contact line owing to the depinning on the 3D surfaces.

For particle aggregation on the surface with nonplanar topography and a structure gradient, we observed that the apex geometry with the asymmetric slope conjugated with the nonwettable material led to the development of directional aggregate characteristics. The sprayed microdroplets tended to spread on the hydrophilic interconnected ipyrawall surfaces (Figure 5A). The particles were homogeneously deposited on the surface (Figure 5B) owing to the concave-shaped contact line formed owing to the pinning effect (Figure 5C). On the hydrophobic interconnected ipyrawall surfaces, the sprayed droplets retained small microdroplets (Figure 5D). During the evaporation process, the microdroplets tended to be trapped in the microcavity with the convex-shaped contact line (Figure 5F) owing to the depinning of evaporating droplets; therefore, the particles directly aggregated in the apex of the microcavity (Figure 5E).

We observed that the directional particle aggregates formed spontaneously on the microcavity surfaces. The effects of the capillary force, low CAH, and geometric structure of the microcavity can lead to the spontaneous motion of the droplet as the droplet volume changes.[31] The continuous volume reduction during droplet evaporation on a hydrophobic substrate facilitated the efficient aggregation of nanoparticles at the bottom or apex of the interconnected microcavity. When sprayed droplets were deposited and evaporated on hydrophobic substrates, the microdroplets reduced in volume while maintaining their quasi-spherical shape in the CCA mode (in Figures 4F and 5F), in contrast to the spreading or wetting observed on hydrophilic substrates in the CCR mode (in Figures 4C and 5C). The droplets evaporated in a manner such that they appeared to slip on the surface owing to the low adhesion forces (i.e., low CAH) and contact line depinning between the droplet and the surface. At the end of the evaporation process, the droplets collapsed, and most particles were deposited within a confined region. Droplet evaporation pulled the particles into the base of the microcavity via capillary force, which limited the transfer of these particle aggregates during subsequent touch. On hydrophilic substrates with high adhesion (i.e., high CAH), the evaporating microdroplets formed at the pinned contact line. After evaporation, depending on the size of sprayed micro-

https://doi.org/10.1021/acsnano.1c01636
ACS Nano 2021, 15, 14049−14060

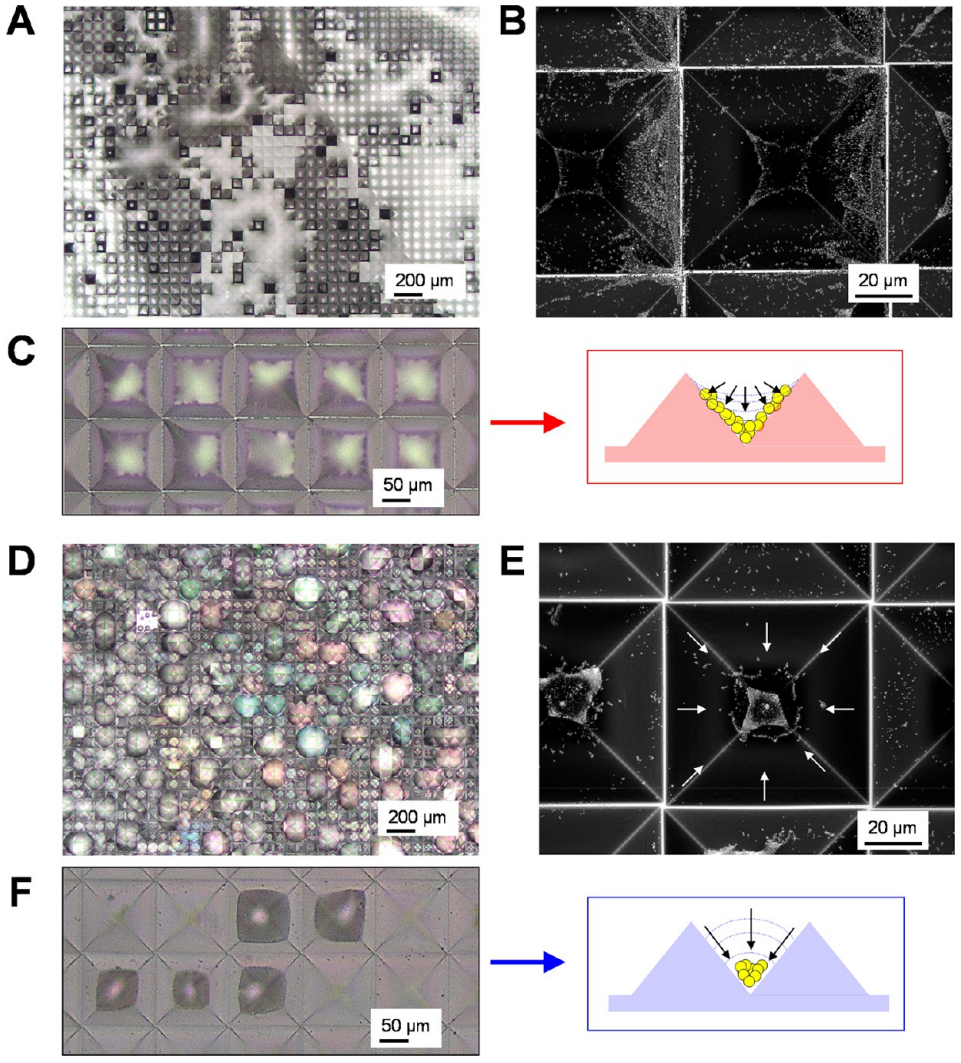

Figure 5. Evaporation process and particle aggregates in the inverted pyramidal wall surfaces (ipyrawall). (A) Spreading of sprayed microdroplets and (B) particle aggregate formation on the hydrophilic ipyrawall. (C) The microdroplets evaporated with the formation of the concave contact line owing to pinning inside the inverted pyramidal cavities. (D) Isolated sprayed microdroplets and (E) particle aggregate formation on the hydrophobic ipyrawall. (F) The microdroplets evaporated with the formation of a convex contact line owing to depinning inside the inverted pyramidal cavities.

droplets, the particles tended to move to the perimeter of the droplet and dispersed homogeneously on the hydrophilic surfaces. We also observed that the effect of the gravitational force on the movement of the evaporating microdroplet was negligible, as shown in Figure S3, as the radius of the microdroplets (≤500 μm) was considerably smaller than the length of the water capillary in the air (~2.7 mm).[32] These results provide insights into the material and surface design and may help to reduce the chances of fomite-based transmission of highly infectious diseases via respiratory droplets in healthcare environments.

To assess whether the microcavity surfaces prevent particle transfer to an intermediate surface by subsequent mechanical contact, we evaluated the particle capture ability of the surfaces (Figure 6). Tape-peeling tests[14] were conducted to evaluate the particle capture stability (see the "Materials and Methods" section and inset in Figure S4C). Both planar and microstructured surfaces were touched and peeled off with tape, and the 3D profile image (Figure 6A) was recorded at the same points to determine the quantity of the residual particles on each surface after contact transfer. After converting the images to a binarized image format, we counted the pixels in these black and white images using MATLAB to estimate the number of transferred particles on the planar and 3D microstructured surfaces (Figures 6B and S4). To quantify the particle capture ability of each surface, the particle capture efficiency (CE) shown in Figure 6C was defined as $1 - (P_1 - P_2)/(P_1 - P_0)$, where P_0, P_1, and P_2 present the pixels of each surface counted before spraying a particle-laden solution, before peeling, and after peeling, respectively (see the "Materials and Methods" section). Figure 6C shows that most aggregated particles were retained on the 3D microcavity surfaces compared to that on planar surfaces (CE: 0.05 and 0.01 for hydrophilic and hydrophobic materials, respectively), indicating that the interconnected microcavity architectures could resist mechanical contact of the tape with the aggregated particles. We also observed that the hydrophobic microcavity (CE: 0.93 for hexawall and 0.96 for ipyrawall) tended to protect more particles than hydrophilic microcavity (CE: 0.89 for hexawall and 0.54 for ipyrawall), which could be attributed to the formation of the directional particle aggregate under capillary force and contact line depinning. Here, the hexawall structures showed a higher

https://doi.org/10.1021/acsnano.1c01636
ACS Nano 2021, 15, 14049−14060

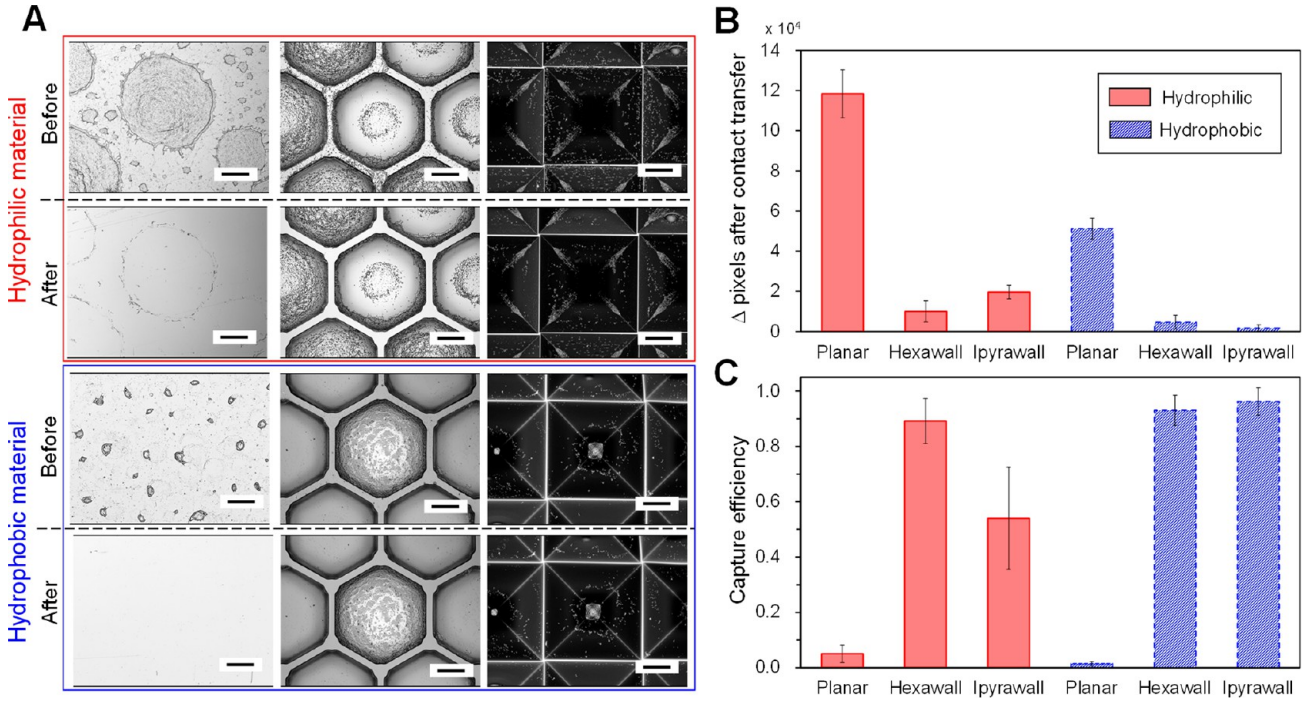

Figure 6. Particle capture efficacy against contact transfer on planar and 3D microstructured surfaces. (A) 3D profile image of the planar and microcavity surfaces before and after the peeling-off test. The scale bars are 100 and 20 μm for the planar and microstructured surfaces, respectively. (B) Differences in the number of pixels counted on the surfaces before peeling and after peeling. (C) Particle capture efficiency calculated from the recorded 3D profile images. Error bars represent standard deviation from the mean (n = 5).

particle CE than the ipyrawall structures in the hydrophilic material. These findings can be explained by the combined effect of the structural gradient of the inverted pyramidal structures and homogeneous particle aggregation on the hydrophilic surface. During the tape-peeling test, the thin tape was slightly deformed under external pressure, which caused the nanoparticles to pull inside the microcavities (refer to Figure 6A and inset in Figure S4C). However, the rigid, interconnected microcavity structures could resist further contact of the tape with the aggregated particles.

While the discussion above provides insights into the capture efficacy of the microcavity surfaces in preventing the transport of the particle aggregates deposited by the respiratory droplets, it does not provide much information on the ability to capture the viral/biological particles ejected by an infected person. For examining the capturing ability of particle aggregates formed from biological fluids, we further investigated the performance of our surface, based on the entrapment of biological materials into the microcavities (Figures 7 and S5−S7). The interconnected microcavity surfaces were sprayed with solutions laden with biological nanoparticles, including adenovirus and extracellular vesicles (EVs) diluted in DI water and PBS, and dried for 30 min under ambient conditions (refer to the "Materials and Methods" section). As shown in Figure 7, the SEM and 3D profile images clearly indicate that the biological nanoparticles were aggregated in the microcavity surfaces, consistent with the findings observed for viruslike nanoparticles (see Figure S5 for additional 3D profile images of adenovirus particle capture on microcavity surfaces). This implies that our microcavity surface had significant potential for reducing the touch transfer of highly infectious agents spread via respiratory droplets.

CONCLUSIONS

In this study, we discussed a comprehensive method to understand the role played by microcavity structures and surface wettability in controlling the aggregation of particle-laden microdroplets to prevent the spread of infectious VPs. For the proof-of-concept, three classes of surfaces, including planar surfaces, and microcavities without and with a structure gradient were fabricated through the UV-NIL process. The interconnected microcavity surfaces were confirmed to provide an overall superior particle CE compared to that provided by planar surfaces owing to the low solid contact area and spatial confinement of sprayed droplets. We also observed that the hydrophobic microcavity surfaces have greater particle capture ability as they enable directional particle aggregation, which is attributed to the slip motion of the microdroplet contact line and capillary force.

However, our study has some limitations. There are differences between virus-laden droplets derived from expiratory ejecta (e.g., saliva) of infected subjects and our simplified particle-laden droplets system. First, the virus-simulant nanoparticles used in this study do not exhibit the mechanical or chemical properties of the viral/biological particles observed in human saliva. In the hydrophilic surface, a coffee ring effect that clearly observed in the viruslike particles (Figures 2D and S7A) was suppressed in the viral/biological particles (Figure S7B,C), which may be attributed to the differences in complex features such as the shape, properties, size, or concentration of the particles and evaporation rate of the particle-laden solution.[35−37] The dried pattern formation of biological fluids would result in additional complexity during the evaporation process due to potential intermolecular interactions that affect particle aggregation and self-assembly.[38,39] As shown in Figure S7, the aggregates of biological particles were larger than that of the

https://doi.org/10.1021/acsnano.1c01636
ACS Nano 2021, 15, 14049−14060

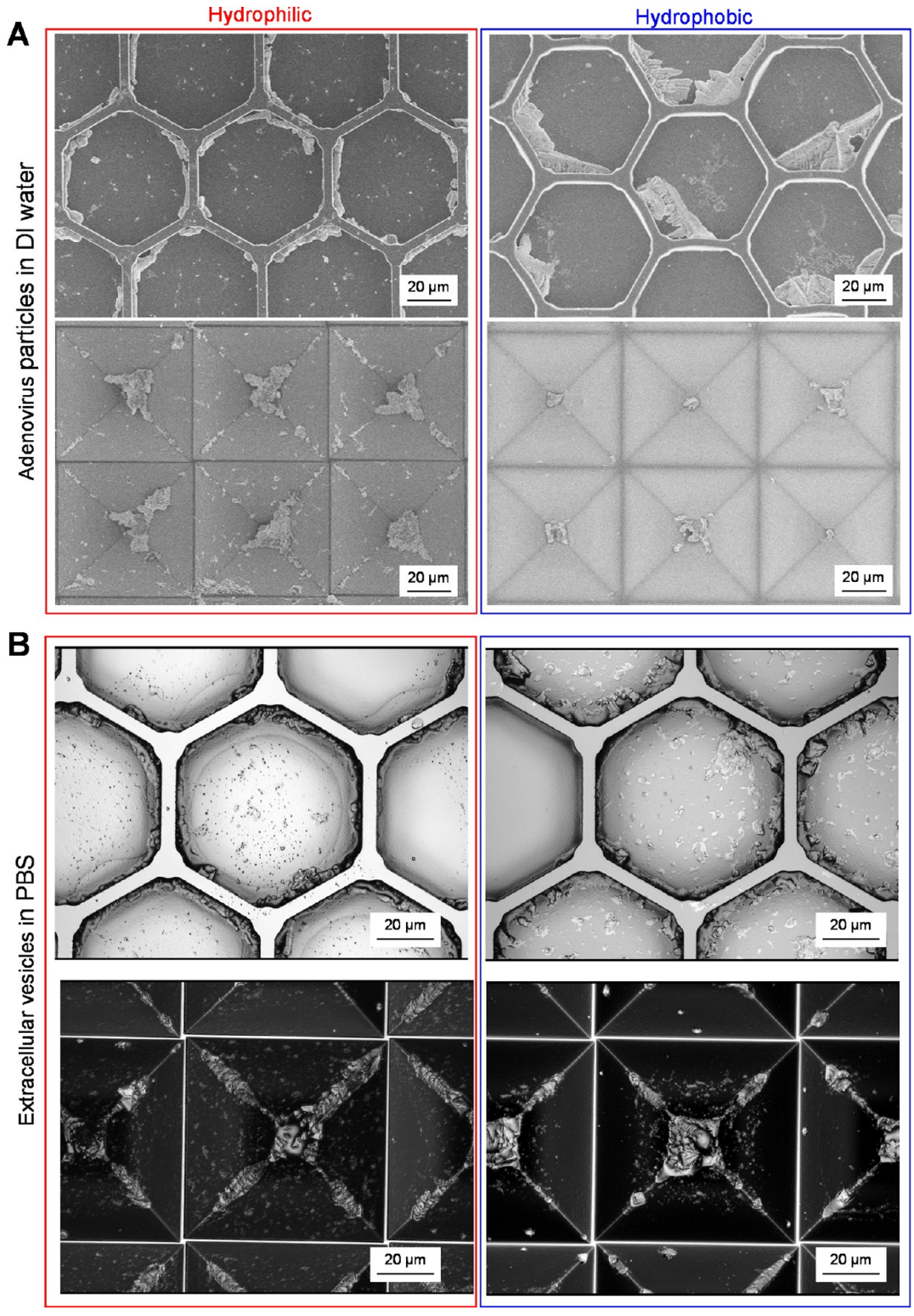

Figure 7. Biological nanoparticle capture on transparent microcavity surfaces. Capture ability of the surface for biological specimens: (A) SEM image of adenovirus particle aggregates; (B) 3D profile image of extracellular vesicles aggregates.

viruslike particles. We speculate that the presence of biological nanoparticles raised the surface energy and interfacial tension of the colloidal solution (that is, a transition of liquid property) on both hydrophilic and hydrophobic surfaces (Figure S8) due to the strong interparticle interaction between biological particles. Consequently, the effective contact area was increased as the initial contact angle of biological particle-laden microdroplets decreased, resulting in larger particle aggregates. Although the viral/biological particles lead to a different form of evaporation-driven particle patterns compared to virus-simulant particles, we still observed a higher concentration of particle aggregates on the hydrophobic surfaces and those confined on the microcavity surfaces, regardless of the particle type (Figures 7, S5, and S7). The investigation of the detailed mechanism of different dried

https://doi.org/10.1021/acsnano.1c01636
ACS Nano 2021, 15, 14049−14060

pattern formation between polymeric and biological particles is beyond the scope of the present study. However, this capturing ability of particle aggregates may be attributed to the fluid dynamics of particle-laden microdroplets described in the manuscript. In addition, it is important to note that PUA and PDMS resins were used as representative materials for the fundamental study to investigate the effect of 3D structures and surface wettability on particle aggregation and touch transfer. From a perspective in structural and material design, we believe that there are plenty of opportunities to control particle aggregation, droplet movement, or surface wettability depending on the types of solutions or solutes. For example, if our structural design for a robust particle capture would be incorporated with advanced surface engineering technologies for implementing superhydrophobic or slippery omniphobic surfaces,[40−43] then we expect that the large aggregates formed due to the presence of biological particles could be concentrated into smaller one. This leads to more efficient particle capture in the microcavity structures. As a proof-of-concept, we coated candle-soot on PUA and PDMS planar surfaces. They showed a contact angle of ∼140 and 170° for EVs-laden droplets, respectively (Figure S8). This supports our expectation that the appropriate surface treatment can lower the surface energy between the biological fluids and substrates. Second, it is clear that DI water and PBS used in this study have different mechanical and chemical properties compared to natural human saliva, yet the present results describing different mixing solutions including artificial saliva (Figures 7, S6A, and S9) may provide a good estimate of the particle aggregate and capture by the evaporation of respiratory virus-laden droplets on different surfaces because the thermophysical properties of saliva are not very different from pure water or particle-laden DI water, NaCl, PBS, or artificial saliva, which were used to mimic the human saliva droplets while maintaining consistency and minimizing the variability in the experiments.[44−47] Therefore, we suggest that future studies should systematically investigate the evaporation-driven aggregates of virus-laden saliva droplets onto the microcavity surfaces under different environmental conditions (e.g., humidity, temperature, and surface wetness).[48−50]

Our findings in this study shed light on the significant potential of the surface chemistry and structural design that can help reduce the possibility of indirect fomite-based transmission of infectious diseases. Considering the diverse biomedical device that require different wettability patterns,[26] microstructured surfaces without structural gradients such as hexawall could be effective in reducing the particle transfer in the hydrophilic material. Conversely, microcavity surfaces with a structure gradient, such as ipyrawall, would be advantageous for designing hydrophobic materials considering the efficient directional particle aggregates and low solid contact area.

The indirect spread of pathogen and infectious diseases from fomites should also be reduced to deal with disease outbreaks. Here, we proposed a robust particle capture surface that allows the directional particle aggregation of microdroplets by controlling the 3D geometry and surface chemistry of the substrate for low contact transfer from the fomites contaminated by respiratory droplets. Although we focused on the low efficacy of transfer from the contaminated microstructured surfaces to other clean surfaces in this study, we expect that the microcavity surfaces will help limit the contact transfer of various pathogens from contaminated objects (i.e., hands) to recipient surfaces due to their small contact area (∼0.21 for hexawall and ∼0.015−0.03 for ipyrawall).[11,17] The efficient particle capturing ability of the microcavity structures not only prevents fomite-based transmission but also may be utilized to preconcentrate target analytes, which may be useful for the environmental monitoring or Raman spectroscopy of pathogens, including SARS-CoV-2.[51−55] In addition to the mechanical and chemical stability of surfaces observed after spray cleaning (Figure S10) and the ability to capture particles even without cleaning (Figures S11−13), our engineered surfaces are highly compatible with large-scale manufacturing techniques.[18,19,30] For example, we have applied a R2R imprinting process to achieve scalable high-throughput fabrication of interconnected microcavity surfaces (Figure 3C). With cost-effective large-scale fabrication, our microstructured surfaces will find a wider range of applications in various fields.

In conclusion, we anticipate that the fabricated surfaces may be one of the primary components in a comprehensive strategy to prevent indirect disease transmission. Since the imprinting performed in this study can be facilitated using a large-area R2R process,[30] in cooperation with existing public health policies, hygiene practices, and pharmaceutical interventions, we believe that the proposed surface technologies can contribute to reducing the spread of pathogens and infectious diseases

MATERIALS AND METHODS

Virus-Simulant Nanoparticles. Polystyrene microspheres (FluoSpheres Carboxylate-Modified Microspheres, 0.2 μm, yellow-green fluorescent (505/515), 2% solids-F8811) were purchased from Thermo Fisher Scientific (Waltham, MA, USA). The nanoparticle was diluted with DI water to ∼10^{11} particles/mL (equivalent to 0.05%) to simulate human saliva containing the VPs.[22,28]

Silicon Mold Fabrication. The hexagonal microwall structures were designed with a wall width of 5 μm, height of 15 μm, and center-to-center distance of 70 μm (the estimated solid fraction of ∼0.21). Si molds were fabricated using photolithography and subsequent reactive ion etching (RIE). The inverted pyramidal microwall structures with α ∼ 125° were also prepared on silicon substrates using a wet etching process. Briefly, the SiN_x/Si wafer was patterned using photolithography in a square lattice, and the patterned wafer with a photoresist was etched using RIE to remove the open nitride layer. Next, the Si wafer was etched using KOH solution at 90 °C. The feature sizes of the microstructures were determined using the designed photomask, and the ridge width of the inverted pyramidal structures could be adjusted by the etching time in the KOH solution. The final Si mold for the inverted pyramidal microwall structures was fabricated with a wall width of ∼0.5−1 μm, depth of ∼50 μm, and center-to-center distance of 70 μm (the estimated solid fraction of ∼0.015−0.03).

Imprinting Process. The microstructures were fabricated using a polyurethane-acrylate (PUA) resin (MINS-311RM resin, Minuta Technology) as a hydrophilic surface and a polydimethylsiloxane resin (PDMS, SYLGARD184) as a hydrophobic surface. The PUA or PDMS resin was dispensed dropwise onto a polyethylene terephthalate (PET) film (125 μm), and the Si mold was pressed slightly against the liquid drops. The PUA and PDMS resins were cured with ultraviolet (UV) light (λ = 365 nm) for a few seconds and in an oven at 100 °C for 1h, respectively. In this study, the microstructured surfaces were replicated using UV nanoimprint lithography as described earlier.[18,19]

Evaporation and Particle Aggregation Tests of Sessile Droplets. The contact angle and diameter on the surfaces were measured using a liquid-droplet analysis tool (SmartDrop, Femtofab Co., Ltd., Korea). A suspension droplet of ∼7 μL was deposited on the planar PUA and PDMS surfaces using the automatic micropipette of the liquid-droplet analysis tool. Once the droplet was deposited on the surface, droplet evaporation was recorded using a liquid-droplet analysis tool equipped with a high-resolution camera. The environmental temperature and relative humidity (RH) were maintained at 25

https://doi.org/10.1021/acsnano.1c01636
ACS Nano 2021, 15, 14049−14060

°C and 10%, respectively. To ensure reproducibility, each experiment was repeated at least three times.

Evaporation and Particle Aggregation Test of Sprayed Microdroplets. The virus-laden droplets expelled during expiratory activities (breathing, speaking, coughing, and sneezing, among others) by infected individuals can deposit and settle on surfaces and objects. These droplets consist of multiple droplets of micrometer and submicrometer diameters (called microdroplets) that vary from 0.05−500 μm with viruses of sizes 20−300 nm.[22,23] To simulate the production of virus-laden microdroplets obtained from expiratory activities, we used a commercial airbrushing system (MONSTER airbrushing kit) to generate an aerosol containing the virus-simulant nanoparticle as shown in Figure S14. An air compressor pressurized the solution up to 3 bar, and the pressurized particle-laden solution was sprayed from the airbrush with a nozzle size of 0.3 mm. The sprayed microdroplet size ranged from few tens of micrometers to hundreds of micrometers in diameter (Figures 2, S2, and S15), which was within the range of the dimension of respiratory microdroplets expelled during coughing, speaking, and breathing.[56−58] The velocity of the sprayed microdroplets at the nozzle was estimated to be approximately 3−5.5 mm/s (corresponding a Weber number of $\ll$1),[59] which was also within the range of the velocity of respiratory exhalation flow.[56,57] In this study, 0.25 or 0.5 mL of the nanoparticle solution was sprayed from the airbrush in 10 or 20 bursts at intervals of 1 s. To investigate the evaporation process and particle aggregation on the surfaces in Figures 2, 4, and 5, we sprayed the particle-laden solutions (0.25 mL) into the air per trial, and the mass deposited from the emitted solution onto each substrate of area $\sim 2 \times 2$ cm^2 was ~9.5 mg (equivalent to ~9−10 μL), as measured using a semimicrobalance (Figure S16). The sprayed microdroplets were evaporated under ambient conditions (~25 °C, RH = 10%).

Size Distribution Analysis. We obtained raw images of sprayed droplets and particle aggregates on hydrophilic and hydrophobic surfaces with an optical microscope (Keyence, VK-X1000). The raw images were imported into ImageJ software, and the background was removed followed by conversion into an 8-bit image and threshold adjustment (Figure S2). This resulted in black and white images. We counted pixels of these black and white images using ImageJ. Considering the limits of the microscopic resolution and the error in image threshold, sprayed droplets and particle aggregates with a diameter less than 5 μm were neglected.

Tape-Peeling Test. Using a protocol adapted from a previous study,[14] a tape-peeling test was performed to quantify the particle capture stability of the 3D microstructured surfaces. For the tape-peeling test (Figure 6), 0.5 mL of a nanoparticle solution was sprayed into the air, and the mass of the microdroplets deposited on each substrate was estimated to be ~19 mg (equivalent to ~18−20 μL). The deposited microdroplets were completely evaporated under ambient conditions (~25 °C, RH 10%) for 30 min. Scotch Magic tape was used for the tape-peeling test and gently pressed using a finger. After gentle separation of the two surfaces, we obtained 3D profile images of the planar and 3D microstructured surfaces at the same points using a laser scanning confocal microscope (Keyence, VK-X1000). The images were converted to a binarized image format with a constant threshold using a home-built MATLAB code, which led to the formation of black and white images. We counted the pixels in these black and white images using MATLAB to estimate the number of particles on the planar and 3D microstructured surfaces. An example of the subsequent image analysis is shown in Figure S3A. However, the accuracy of the estimation of the number of particles on 3D microstructured surfaces is limited compared to that of 2D planar surfaces. To minimize the inaccuracy of the estimation of the number of transferred particles after the tape-peeling test, the transfer efficiency (TE) of particle aggregates was defined as $(P_1 - P_2)/(P_1 - P_0)$ (Figure S4D), and the corresponding CE was defined as 1 − TE. Here, P_0, P_1, and P_2 are the pixels of surfaces counted before spraying of a particle-laden solution, before peeling, and after peeling, respectively.

Adenovirus Test. A replication-defective and purified adenovirus with a VP concentration of >10^{12} VP/mL was purchased from VectorBuilder (VB150925−10024; Chicago, IL, USA). The diameter of the adenovirus particles used here ranged from 0.07 to 0.1 μm. The adenovirus sample was diluted in DI water to obtain an experimental concentration of >10^{11} VP/mL. An adenovirus solution (0.25 mL) was sprayed onto the surfaces and then fully dried under ambient conditions for 30 min in a biological safety fume hood. Last, VP aggregation on the surfaces was assessed using a laser scanning confocal microscope (Keyence, VK-X1000).

EV Test. Lung-derived EVs, which are biogenic nanoparticles (~10^9/mL) with a particle size ranging from 0.05 to 0.5 μm (Figure S17), were purified from bronchoalveolar lavage fluid collected from mice, as described previously.[60] The EVs were diluted to a concentration of ~10^9/mL in PBS (Gibco PBS 1×, pH 7.4). The success of the EV isolation process was verified using FE-SEM. Next, the EV solution (0.05 mL) was sprayed onto the surfaces and completely dried under ambient conditions for 30 min. Last, particle aggregation on the surfaces was evaluated using a laser scanning confocal microscope (Keyence, VK-X1000).

Optical Transmission. The light transmission spectra of the samples were recorded between 300 and 700 nm using a UV/vis/NIR spectrophotometer (V-670 Spectrophotometer, JASCO) with an integrating sphere attachment.

ASSOCIATED CONTENT

Supporting Information

The Supporting Information is available free of charge at https://pubs.acs.org/doi/10.1021/acsnano.1c01636.

Evaporation dynamics of sessile droplets, SEM images, representative images of size distribution analysis, gravitational effects on the particle aggregation in the interconnected microcavity surfaces, tape-peeling tests, 3D profile images, particle aggregation data, surface treatment methods, chemical and mechanical stabilities of hydrophilic and hydrophobic microcavity surfaces, evaporation of sprayed droplets, stable particle capture of hydrophilic and hydrophobic microcavity surfaces, optical images of the particle aggregates, weight evolution of sessile and sprayed droplets, additional references (PDF)

AUTHOR INFORMATION

Corresponding Author

Young Tae Cho − *Department of Mechanical Engineering and Department of Smart Manufacturing Engineering, Changwon National University, Changwon 51140, South Korea;* orcid.org/0000-0001-7545-4646; Email: ytcho@changwon.ac.kr

Authors

Seok Kim − *Department of Mechanical Engineering and Department of Smart Manufacturing Engineering, Changwon National University, Changwon 51140, South Korea;* orcid.org/0000-0002-6049-6461

Woo Young Kim − *Department of Smart Manufacturing Engineering, Changwon National University, Changwon 51140, South Korea*

Sang-Hoon Nam − *Department of Mechanical Engineering, Massachusetts Institute of Technology, Cambridge, Massachusetts 02139, United States*

Seunghang Shin − *Department of Smart Manufacturing Engineering, Changwon National University, Changwon 51140, South Korea*

Su Hyun Choi − *Department of Mechanical Engineering, Changwon National University, Changwon 51140, South Korea*

Do Hyeog Kim − *Department of Mechanical Engineering, Changwon National University, Changwon 51140, South Korea*
Heedoo Lee − *Department of Biology and Chemistry, Changwon National University, Changwon 51140, South Korea*
Hyeok Jae Choi − *Department of Biology and Chemistry, Changwon National University, Changwon 51140, South Korea*
Eungman Lee − *Department of Radiation Oncology, College of Medicine, Ewha Womans University, Seoul 07804, South Korea*
Jung-Hyun Park − *Department of Molecular Medicine, College of Medicine, Ewha Womans University, Seoul 07804, South Korea*
Inho Jo − *Department of Molecular Medicine, College of Medicine, Ewha Womans University, Seoul 07804, South Korea; Ewha Education & Research Center for Infection, Ewha Womans University Medical Center, Seoul 07804, South Korea*
Nicholas X. Fang − *Department of Mechanical Engineering, Massachusetts Institute of Technology, Cambridge, Massachusetts 02139, United States*

Complete contact information is available at: https://pubs.acs.org/10.1021/acsnano.1c01636

Notes

The authors declare no competing financial interest.

ACKNOWLEDGMENTS

The authors are grateful for several sources of support. S.K., W.Y.K., S.S., S.H.C., D.H.K., Y.T.C., S.H.N., and N.X.F. acknowledge support from the Technology Innovation Program (20007064, Realization of air cleaning mobility HAMA (superHydrophobic Additive Manufactured Air cleaner) Project) and Industrial Technology Innovation Program (20000665, Development of ecofriendly and highly durable surface treatment for superomniphobic substrate on the large area over 4 m^2) funded by the Ministry of Trade, Industy & Energy (MOTIE, Korea). S.K., W.Y.K., S.S., S.H.C., D.H.K., and Y.T.C. acknowledge support from the National Research Foundation of Korea (NRF) grant funded by the Korea government (MSIT) (NRF-2019R1A5A8083201). S.K. acknowledges support from the National Research Foundation of Korea (NRF) grant funded by the Korea government (MSIT) (NRF-2020R1G1A1101420).

REFERENCES

(1) World Health Organization. *Transmission of SARS-CoV-2: Implications for Infection Prevention Precautions*; WHO: Geneva, 2020. https://www.who.int/news-room/commentaries/detail/transmission-of-sars-cov-2-implications-for-infection-prevention-precautions [accessed June 2021].
(2) Lewis, D. COVID-19 Rarely Spreads through Surfaces. So Why Are We Still Deep Cleaning? *Nature* **2021**, *590* (7844), 26−28.
(3) Azimi, P.; Keshavarz, Z.; Cedeno Laurent, J. G.; Stephens, B.; Allen, J. G. Mechanistic Transmission Modeling of COVID-19 on the Diamond Princess Cruise Ship Demonstrates the Importance of Aerosol Transmission. *Proc. Natl. Acad. Sci. U. S. A.* **2021**, *118* (8), e2015482118.
(4) Van Doremalen, N.; Bushmaker, T.; Morris, D. H.; Holbrook, M. G.; Gamble, A.; Williamson, B. N.; Tamin, A.; Harcourt, J. L.; Thornburg, N. J.; Gerber, S. I.; et al. Aerosol and Surface Stability of SARS-CoV-2 as Compared with SARS-CoV-1. *N. Engl. J. Med.* **2020**, *382* (16), 1564−1567.
(5) Xiao, S.; Li, Y.; Wong, T. W.; Hui, D. S. Role of Fomites in SARS Transmission during the Largest Hospital Outbreak in Hong Kong. *PLoS One* **2017**, *12*, No. e0181558.
(6) Xie, C.; Zhao, H.; Li, K.; Zhang, Z.; Lu, X.; Peng, H.; Wang, D.; Chen, J.; Zhang, X.; Wu, D.; Gu, Y.; Yuan, J.; Zhang, L.; Lu, J. The Evidence of Indirect Transmission of SARS-CoV-2 Reported in Guangzhou, China. *BMC Public Health* **2020**, *20*, 1202.
(7) Kraay, A. N.; Hayashi, M. A.; Hernandez-Ceron, N.; Spicknall, I. H.; Eisenberg, M. C.; Meza, R.; Eisenberg, J. N. S. Fomite-Mediated Transmission as a Sufficient Pathway: A Comparative Analysis across Three Viral Pathogens. *BMC Infect. Dis.* **2018**, *18*, 540.
(8) Chin, A. W.; Poon, L. L. Stability of SARS-CoV-2 in Different Environmental Conditions-Authors' Reply. *Lancet Microbe* **2020**, *1* (4), No. e146.
(9) Chia, P. Y.; Coleman, K. K.; Tan, Y. K.; Ong, S. W. X.; Gum, M.; Lau, S. K.; Lim, X. F.; Lim, A. S.; Sutjipto, S.; Lee, P. H.; Son, T. T.; Young, B. E.; Milton, D. K.; Gray, G. C.; Schuster, S.; Barkham, T.; De, P. P.; Vasoo, S.; Chan, M.; Ang, B. S. P.; et al. Detection of Air and Surface Contamination by SARS-CoV-2 in Hospital Rooms of Infected Patients. *Nat. Commun.* **2020**, *11* (1), 1−7.
(10) Bloise, I.; Gomez-Arroyo, B.; Garcia-Rodriguez, J. Detection of SARS-CoV-2 on High-Touch Surfaces in a Clinical Microbiology Laboratory. *Journal of Hospital infection* **2020**, *105* (4), 784−786.
(11) Liu, Q.; Brookbank, L.; Ho, A.; Coffey, J.; Brennan, A. B.; Jones, C. J. Surface Texture Limits Transfer of *S. aureus*, T4 Bacteriophage, Influenza B Virus and Human Coronavirus. *PLoS One* **2020**, *15*, No. e0244518.
(12) Goldman, E. Exaggerated Risk of Transmission of COVID-19 by Fomites. *Lancet Infect. Dis.* **2020**, *20* (8), 892−893.
(13) Boone, S. A.; Gerba, C. P. Significance of Fomites in the Spread of Respiratory and Enteric Viral Disease. *Appl. Environ. Microbiol.* **2007**, *73*, 1687−1696.
(14) Wang, D.; Sun, Q.; Hokkanen, M. J.; Zhang, C.; Lin, F.-Y.; Liu, Q.; Zhu, S.-P.; Zhou, T.; Chang, Q.; He, B.; et al. Design of Robust Superhydrophobic Surfaces. *Nature* **2020**, *582*, 55−59.
(15) Zhang, N.; Jia, W.; Wang, P.; King, M.-F.; Chan, P.-T.; Li, Y. Most Self-Touches Are with the Nondominant Hand. *Sci. Rep.* **2020**, *10*, 10457.
(16) Zhang, N.; Wang, P.; Miao, T.; Chan, P.-T.; Jia, W.; Zhao, P.; Su, B.; Chen, X.; Li, Y. Real Human Surface Touch Behavior Based Quantitative Analysis on Infection Spread *via* Fomite Route in an Office. *Building and Environment* **2021**, *191*, 107578.
(17) Imani, S. M.; Maclachlan, R.; Rachwalski, K.; Chan, Y.; Lee, B.; McInnes, M.; Grandfield, K.; Brown, E. D.; Didar, T. F.; Soleymani, L. Flexible Hierarchical Wraps Repel Drug-Resistant Gram-Negative and Positive Bacteria. *ACS Nano* **2020**, *14* (1), 454−465.
(18) Kim, S.; Kim, D. H.; Choi, S. H.; Kim, W. Y.; Kwon, S.; Cho, Y. T. Effect of Surface Pattern Morphology on Inducing Superhydrophobicity. *Appl. Surf. Sci.* **2020**, *513*, 145847.
(19) Choi, S. H.; Kim, D. H.; Kim, S.; Kim, W. Y.; Kim, S.; Cho, Y. T. Tulip-Shaped Pattern Imprinting for Omni-Phobic Surfaces Using Partially Cured Photopolymer. *Appl. Sci.* **2021**, *11*, 1747.
(20) Zhu, P.; Kong, T.; Tang, X.; Wang, L. Well-Defined Porous Membranes for Robust Omniphobic Surfaces *via* Microfluidic Emulsion Templating. *Nat. Commun.* **2017**, *8*, 15823.
(21) Chiam, Z.; Song, X. P.; Lai, H. R.; Tan, H. T. W. Particulate Matter Mitigation *via* Plants: Understanding Complex Relationships with Leaf Traits. *Sci. Total Environ.* **2019**, *688*, 398−408.
(22) Anand, S.; Mayya, Y. S. Size Distribution of Virus Laden Droplets from Expiratory Ejecta of Infected Subjects. *Sci. Rep.* **2020**, *10*, 21174.
(23) Castano, N.; Cordts, S. C.; Kurosu Jalil, M.; Zhang, K. S.; Koppaka, S.; Bick, A. D.; Paul, R.; Tang, S. K. Y. Fomite Transmission, Physicochemical Origin of Virus-Surface Interactions, and Disinfection Strategies for Enveloped Viruses with Applications to SARS-CoV-2. *ACS Omega* **2021**, *6*, 6509−6527.

(24) Dai, H.; Dong, Z.; Jiang, L. Directional Liquid Dynamics of Interfaces with Superwettability. *Science Advances* **2020**, *6* (37), No. eabb5528.
(25) Zhang, T. Y.; Mou, L. W.; Zhang, Y. C.; Zhang, J. Y.; Li, J. Q.; Fan, L. W. Hierarchical Microcavity Topography for Enhancement of Water Vapor Condensation Heat Transfer by Regulating Droplet Dynamics and Droplet Size Distribution. *Case Studies in Thermal Engineering* **2021**, *24*, 100882.
(26) Han, T.; Noh, H.; Park, H. S.; Kim, M. W. Effects of Wettability on Droplet Movement in a V-Shaped Groove. *Sci. Rep.* **2018**, *8*, 16013.
(27) Lustig, S. R.; Biswakarma, J. J. H.; Rana, D.; Tilford, S. H.; Hu, W.; Su, M.; Rosenblatt, M. S. Effectiveness of Common Fabrics to Block Aqueous Aerosols of Virus-Like Nanoparticles. *ACS Nano* **2020**, *14*, 7651−7658.
(28) Pan, Y.; Zhang, D.; Yang, P.; Poon, L. L. M.; Wang, Q. Viral Load of SARS-CoV-2 in Clinical Samples. *Lancet Infect. Dis.* **2020**, *20*, 411−412.
(29) Orejon, D.; Sefiane, K.; Shanahan, M. E. R. Stick-Slip of Evaporating Droplets: Substrate Hydrophobicity and Nanoparticle Concentration. *Langmuir* **2011**, *27*, 12834−12843.
(30) Cho, Y. T.; Kwon, S.; Seo, J. W.; Kim, J. G.; Cho, J. W.; Park, J. W.; Kim, H.; Lee, S. Development of Large Area Nano Imprint Technology by Step and Repeat Process and Pattern Stitching Technique. *Microelectron. Eng.* **2009**, *86*, 2417−2422.
(31) Xu, W.; Lan, Z.; Peng, B.; Wen, R.; Chen, Y.; Ma, X. Directional Movement of Droplets in Grooves: Suspended or Immersed? *Sci. Rep.* **2016**, *6*, 1−11.
(32) Park, K.-C.; Kim, P.; Grinthal, A.; He, N.; Fox, D.; Weaver, J. C.; Aizenberg, J. Condensation on Slippery Asymmetric Bumps. *Nature* **2016**, *531*, 78−82.
(33) Intartaglia, R.; Beke, S.; Moretti, M.; De Angelis, F.; Diaspro, A. Fast and Cost-Effective Fabrication of Large-Area Plasmonic Transparent Biosensor Array. *Lab Chip* **2015**, *15*, 1343−1349.
(34) Helmer, D.; Keller, N.; Kotz, F.; Stolz, F.; Greiner, C.; Nargang, T. M.; Sachsenheimer, K.; Rapp, B. E. Transparent, Abrasion-Insensitive Superhydrophobic Coatings for Real-World Applications. *Sci. Rep.* **2017**, *7*, 1−6.
(35) Yunker, P. J.; Still, T.; Lohr, M. A.; Yodh, A. G. Suppression of the Coffee-Ring Effect by Shape-Dependent Capillary Interactions. *Nature* **2011**, *476* (7360), 308−311.
(36) Mampallil, D.; Eral, H. B. A Review on Suppression and Untilization of the Coffee-Ring Effect. *Adv. Colloid Interface Sci.* **2018**, *252*, 38−54.
(37) Gorr, H. M.; Zueger, J. M.; Barnard, J. A. Lysozyme Pattern Formation in Evaporating Drops. *Langmuir* **2012**, *28* (9), 4039−4042.
(38) Carreón, Y. J.P.; González-Gutiérrez, J.; Pérez-Camacho, M. I.; Mercado-Uribe, H. Patterns Produced by Dried Droplets of Protein Binary Mixtures Suspended in Water. *Colloids Surf., B* **2018**, *161*, 103−110.
(39) Pal, A.; Gope, A.; Athair, A. S.; Iannacchione, G. S. A Comparative Study of the Drying Evolution and Dried Morphology of Two Globular Proteins in De-Ionized Water Solutions. *RSC Adv.* **2020**, *10* (29), 16906−16916.
(40) Deng, X.; Mammen, L.; Butt, H.-J.; Vollmer, D. Candle Soot as a Template for a Transparent Robust Superamphiphobic Coating. *Science* **2012**, *335* (6064), 67−70.
(41) Wang, L.; McCarthy, T. J. Covalently Attached Liquids: Instant Omniphobic Surfaces with Unprecedented Repellency. *Angew. Chem.* **2016**, *128*, 252−256.
(42) Yang, S.; Dai, X.; Stogin, B. B.; Wong, T.-S. Ultrasensitive Surface-Enhanced Raman Scattering Detection in Common Fluids. *Proc. Natl. Acad. Sci. U. S. A.* **2016**, *113* (2), 268−273.
(43) Czolkos, I.; Hakonen, B.; Orwar, O.; Jesorka, A. High-Resolution Micropatterned Teflon AF Substrates for Biocompatible Nanofluidic Devices. *Langmuir* **2012**, *28* (6), 3200−3205.
(44) Chaudhuri, S.; Basu, S.; Kabi, P.; Unni, V. R.; Saha, A. Modeling the Role of Respiratory Droplets in Covid-19 Type Pandemics. *Phys. Fluids* **2020**, *32* (6), 063309.
(45) Bhardwaj, R.; Agrawal, A. Tailoring Surface Wettability to Reduce Chances of Infection of COVID-19 by a Respiratory Droplet and to Improve the Effectiveness of Personal Protection Equipment. *Phys. Fluids* **2020**, *32* (8), 081702.
(46) Bhardwaj, R.; Agrawal, A. Likelihood of Survival of Coronavirus in a Respiratory Droplet Deposited on a Solid Surface. *Phys. Fluids* **2020**, *32* (6), 061704.
(47) Sharma, S.; Pinto, R.; Saha, A.; Chaudhuri, S.; Basu, S. On Secondary Atomization and Blockage of Surrogate Cough Droplets in Single and Multilayer Face Masks. *Science Advances* **2021**, *7* (10), No. eabf0452.
(48) Zhao, P.; Li, Y.; Tsang, T. L.; Chan, P. T. Equilibrium of Particle Distribution on Surfaces Due to Touch. *Building and Environment* **2018**, *143*, 461−472.
(49) Zhao, P.; Chan, P. T.; Gao, Y.; Lai, H. W.; Zhang, T.; Li, Y. Physical Factors that Affect Microbial Transfer during Surface Touch. *Building and Environment* **2019**, *158*, 28−38.
(50) Zhao, P.; Li, Y. Modeling and Experimental Validation of Microbial Transfer *via* Surface Touch. *Environ. Sci. Technol.* **2021**, *55* (7), 4148−4161.
(51) Chi, J.; Zhang, X.; Wang, Y.; Shao, C.; Shang, L.; Zhao, Y. Bio-Inspired Wettability Patterns for Biomedical Applications. *Mater. Horiz.* **2021**, *8*, 124−144.
(52) Kim, Y.; Jung, K.; Chang, J.; Kwak, T.; Lim, Y.; Kim, S.; Na, J.; Lee, J.; Choi, I.; Lee, L. P.; Kim, D.; Kang, T. Active Surface Hydrophobicity Switching and Dynamic Interfacial Trapping of Microbial Cells by Metal Nanoparticles for Preconcentration and In-Plane Optical Detection. *Nano Lett.* **2019**, *19*, 7449−7456.
(53) De Angelis, F.; Gentile, F.; Mecarini, F.; Das, G.; Moretti, M.; Candeloro, P.; Coluccio, M. L.; Cojoc, G.; Accardo, A.; Liberale, C.; Zaccaria, R. P.; Perozziello, G.; Tirinato, L.; Toma, A.; Cuda, G.; Cingolani, R.; Di Fabrizio, E. Breaking the Diffusion Limit with Super-Hydrophobic Delivery of Molecules to Plasmonic Nanofocusing SERS Structures. *Nat. Photonics* **2011**, *5*, 682−687.
(54) Yang, S.; Dai, X.; Stogin, B. B.; Wong, T. S. Ultrasensitive Surface-Enhanced Raman Scattering Detection in Common Fluids. *Proc. Natl. Acad. Sci. U. S. A.* **2016**, *113* (2), 268−273.
(55) Tadesse, L. F.; Ho, C. S.; Chen, D. H.; Arami, H.; Banaei, N.; Gambhir, S. S.; Jeffrey, S. S.; Saleh, A. A. E.; Dionne, J. Plasmonic and Electrostatic Interactions Enable Uniformly Enhanced Liquid Bacterial Surface-Enhanced Raman Scattering (SERS). *Nano Lett.* **2020**, *20* (10), 7655−7661.
(56) Xie, X.; Li, Y.; Chwang, A. T. Y.; Ho, P. L.; Seto, W. H. How Far Droplets Can Move in Indoor Environments-Revisiting the Wells Evaporation-Falling Curve. *Indoor Air* **2007**, *17* (3), 211−225.
(57) Dbouk, T.; Drikakis, D. On Coughing and Airborne Droplet Transmission to Humans. *Phys. Fluids* **2020**, *32* (5), 053310.
(58) Fedorenko, A.; Grinberg, M.; Orevi, T.; Kashtan, N. Survival of Enveloped Bacteriophage Phi6 (A Surrogate for SARS-CoV-2) in Evaporated Saliva Microdroplets Deposited on Glass Surfaces. *Sci. Rep.* **2020**, *10* (1), 1−10.
(59) Levitsky, I.; Tavor, D. Improved Atomization *via* a Mechanical Atomizer with Optimal Geometric Parameters and an Air-Assisted Component. *Micromachines* **2020**, *11*, 584.
(60) Lee, H.; Groot, M.; Pinilla-Vera, M.; Fredenburgh, L. E.; Jin, Y. Identification of miRNA-Rich Vesicles in Bronchoalveolar Lavage Fluid: Insights into the Function and Heterogeneity of Extracellular Vesicles. *J. Controlled Release* **2019**, *294*, 43−52.

https://doi.org/10.1021/acsnano.1c01636
ACS Nano 2021, 15, 14049−14060